Petroleum coke-derived porous carbon encapsulating phase change materials for solar-thermal-electricity output

View Online   Export Citation   CrossMark

Jianhua Bian, [iD] Lili Wang,[a) [iD] Libing Liao, [iD] and Guocheng Lv[a) [iD]

AFFILIATIONS

Engineering Research Center of Ministry of Education for Geological Carbon Storage and Low Carbon Utilization of Resources, Beijing Key Laboratory of Materials Utilization of Nonmetallic Minerals and Solid Wastes, National Laboratory of Mineral Materials, Hebei Key Laboratory of Resource Low-carbon Utilization and New Materials, School of Materials Science and Technology, China University of Geosciences (Beijing), Beijing 100083, China

[a)]Authors to whom correspondence should be addressed: wanglily@ustc.edu.cn and guochenglv@cugb.edu.cn

ABSTRACT

Solar energy utilization is hindered by intermittency, highlighting the urgency of advanced thermal energy storage technologies. Phase change materials (PCMs) are promising candidates but suffer from leakage and poor photothermal performance. Herein, we fabricate hierarchically porous carbon (PCPC) from petroleum coke (a refinery by-product) via a salt-templating method, which serves as an efficient support for paraffin wax (PW) PCMs. Benefiting from the unique porous structure of PCPC, the resulting form-stable composite PCM (PW/PCPC) exhibits remarkable performance, including a high latent heat of $134.4\,\mathrm{J\,g^{-1}}$, excellent structural stability, and outstanding cycling durability. Simultaneously, the composite realizes an outstanding photothermal conversion efficiency of 89.68%. A key breakthrough is the development of an integrated solar-thermal-electricity conversion system by combining PW/PCPC with a commercial thermoelectric generator. This system delivers a stable power output density of $7.01\,\mathrm{W\,m^{-2}}$ and can continuously generate electricity using stored thermal energy even after light source removal. This work not only provides a waste valorization strategy for high-performance composite PCMs but also demonstrates their great potential in efficient solar energy harvesting and sustainable power supply, addressing critical challenges in solar energy utilization.

Published under an exclusive license by AIP Publishing. https://doi.org/10.1063/5.0312880

The rapid advancement of technology has led to a substantial consumption of traditional fossil fuels.[1–4] To address the ever-increasing global energy demand and mitigate the associated environmental pressures, green and sustainable clean energy sources, particularly solar energy, have garnered considerable interest.[5] However, the inherent intermittency, instability, and seasonal variability of solar energy pose major obstacles to its large-scale application.[6] Consequently, the development of efficient and sustainable energy storage and conversion technologies has emerged as a critical research frontier.[7–9] In this context, phase change materials (PCMs), which utilize reversible phase transitions, offer a promising solution for addressing the challenge of intermittent energy supply.[10,11]

Organic solid–liquid PCMs represent ideal media for thermal energy storage due to their high energy storage density (latent heat) and near-isothermal phase transition behavior, finding potential applications in solar energy utilization and industrial waste heat recovery.[12] Nevertheless, the broad practical adoption of these materials is significantly hampered by several inherent drawbacks, including leakage in the liquid state, poor thermal conductivity, and a general lack of photo-responsive properties.[13,14] Therefore, it is crucial to develop effective encapsulation and functionalization strategies for organic PCMs to overcome these limitations.[15–17]

Constructing shape-stable composite PCMs using porous materials as supporting matrices has proven effective in preventing leakage.[18,19] Among various porous materials, porous carbon stands out owing to its high specific surface area, tunable pore structure, excellent chemical stability, and favorable thermal conductivity.[20] However, many high-performance porous carbons, such as graphene aerogels,[21,22] carbon nanotube sponges,[23,24] and metal–organic framework (MOF)-derived carbons,[25,26] are often hampered by complex synthesis procedures and high raw material costs, which limits their large-scale practical application. In contrast, porous carbons derived from biomass waste offer a sustainable and cost-effective alternative, simultaneously enabling waste recycling and reduced environmental impact.[27]

For instance, Moulakhnif *et al.* fabricated porous carbon from *Capparis spinosa* waste via carbonization for PCM encapsulation and achieved a loading capacity of 45 wt. % with stable performance.[28] Wang *et al.* developed a composite PCM based on bamboo shoot-derived carbon, reaching an encapsulation efficiency of 60.47%.[29] Similarly, Luo *et al.* reported a composite PCM using garlic peel-derived carbon that maintained good stability over 200 thermal cycles.[11] Although biomass-derived porous carbon-based composite PCMs have garnered increasing research interest, current investigations remain predominantly focused on encapsulation and thermal conductivity enhancement. However, their potential in energy conversion applications, particularly for integrated photothermal conversion and storage, remains underexplored and insufficient to meet developing demands.[30]

In this work, a porous carbon scaffold (PCPC) was constructed from petroleum coke (PC), a by-product of oil refining, using a NaCl templating method combined with a phenolic resin binder. Paraffin wax (PW) was subsequently encapsulated into the PCPC through vacuum impregnation to yield the composite PCM (PW/PCPC). The resulting PW/PCPC composite PCM exhibits high latent heat of $134.4 \, J \, g^{-1}$, along with excellent stability and remarkable cycling durability. More notably, the composite demonstrates outstanding photothermal conversion performance, achieving an efficiency of 89.68%. Furthermore, a solar-thermal-electricity conversion system was fabricated by integrating the composite PCM with a commercial thermoelectric generator (TEG). This system enables continuous solar energy harvesting and stable power output, which achieved a power density of $7.01 \, W \, m^{-2}$. This work thus establishes a promising pathway for solar energy utilization and clean power supply.

Figure 1(a) schematically illustrates the detailed preparation procedures for the PCPC and PW/PCPC composites. Figures 1(b)–1(d) present the morphological characteristics of the PCPC scaffold. It is

evident that the loose petroleum coke particles are bonded together via the curing and cross-linking of phenolic resin. After water washing to remove the NaCl template, a three-dimensional (3D) open-cell structure emerges within the PCPC. With the increase in the dosage of NaCl porogen, the internal structure of the PCPC becomes progressively more porous. However, constrained by the particle size of NaCl, the internal pore size remains essentially at the micrometer scale. Following vacuum impregnation, PW completely infiltrates the pores of the PCPC, as shown in Figs. 1(e) and 1(f). This effective encapsulation is primarily due to capillary action and van der Waals forces.

The XRD patterns of NaCl, PC, and PCPC are presented in Fig. 2(a). Two broad diffraction peaks are observed at $2\theta = 25°$ and $43°$, corresponding to the (002) and (100) planes of amorphous carbon, respectively.[31] Compared with PC, the PCPC pattern exhibits a broader diffraction peak at $2\theta = 25°$ and only a slight intensity increase at $2\theta = 43°$. This suggests that the carbonization process promoted the growth of graphite microcrystals, thereby resulting in a more disordered PCPC structure.[32] The absence of any NaCl peaks in the XRD pattern indicates the complete removal of the NaCl template from PCPC. Figure 2(b) shows the pore size distribution and porosity of PCPC. Taking $PCPC_7$ as an example, the internal pore diameters range from 1.6 to $362 \, \mu m$, with pores below $52 \, \mu m$ accounting for 90% of the total. The measured porosities of the PCPC samples were 75.66%, 77.88%, and 78.68%. This high porosity enables PCPC to possess sufficient load capacity for PCM. Meanwhile, it can be observed that the compressive strength of PCPC decreases with the increase in template content [Fig. 2(c)]. This is because the increase in template agent content results in looser connections between internal petroleum coke particles in PCPC, which further forms more and larger pores in PCPC (Fig. S1), thereby reducing the overall compressive strength of porous carbon.[33] As shown in Fig. 2(d), PCPC exhibited excellent hydrophobicity, with water contact angles of 114.52°, 120.38°, and 125.70°, all
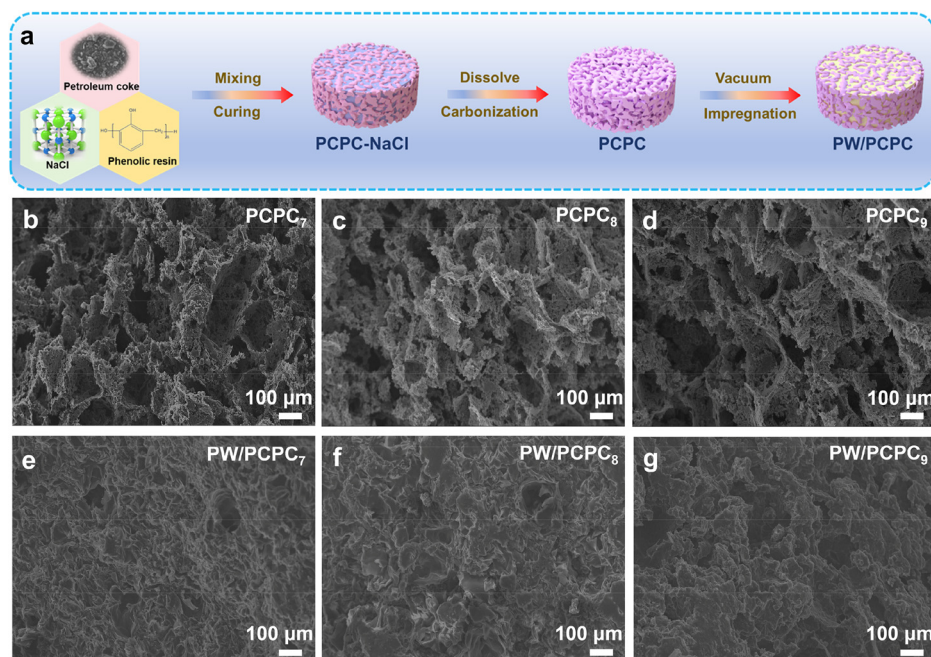

FIG. 1. (a) Schematic illustration of the preparation of PCPC and PW/PCPC. (b)–(d) SEM images of $PCPC_7$, $PCPC_8$, and $PCPC_9$. (b)–(d) SEM images of PW/$PCPC_7$, PW/$PCPC_8$, and PW/$PCPC_9$.
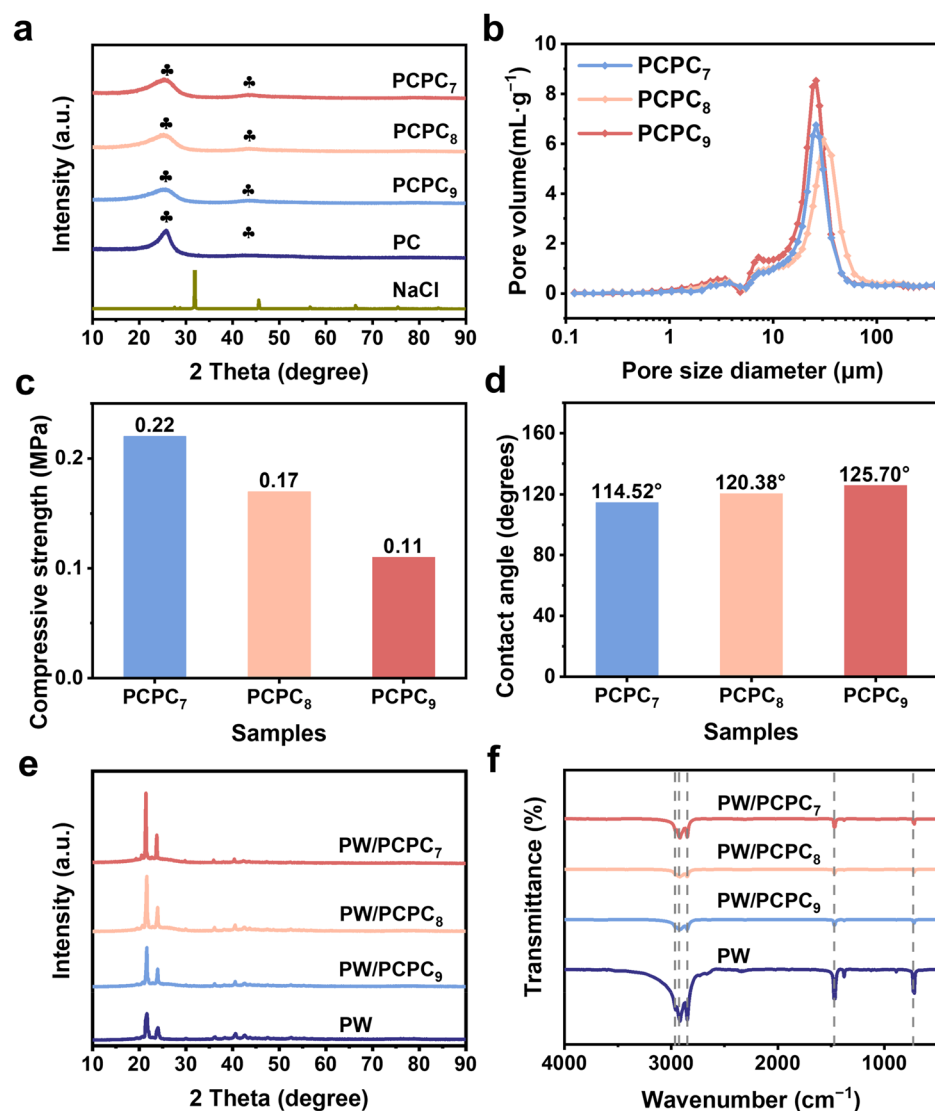
FIG. 2. (a) XRD patterns of NaCl, PC, and PCPC. (b) Aperture distribution curves of PCPC. (c) Compressive strength of PCPC. (d) Water contact angles of PCPC. XRD patterns (e) and FTIR spectrum (f) of PW and PW/PCPC.

exceeding 110°. The enhanced hydrophobicity of PCPC was attributed to the increase in NaCl, which led to greater surface roughness of PCPC. This observation aligns with the Wenzel model, which posits a positive correlation between the material hydrophobicity and the surface roughness.[34]

Figure 2(e) displays the XRD patterns of pure PW and the PW/PCPC composite. The characteristic peaks of PW at $2\theta = 21.4°$ and $23.7°$ correspond to the (110) and (200) crystallographic planes of PW crystals.[35] Due to the high loading ratio of PW, only the characteristic peaks of PW are observed in the PW/PCPC composite. The absence of any additional peaks indicates a purely physical interaction between PCPC and PW. The intensity of the characteristic diffraction peaks of PW crystals in the PW/PCPC composite is higher than that of pure PW, suggesting that the encapsulation within PCPC facilitates the crystallization of PW.[36] The FTIR spectra of PW and PW/PCPC are shown in Fig. 2(f). The characteristic peaks of PW at 2915 and

$2855 \, cm^{-1}$ are attributed to the symmetric stretching vibrations of the $-CH_3$ and $-CH_2$ groups, respectively, while the peaks at 1468 and $715 \, cm^{-1}$ correspond to the deformation vibrations of the $-CH_3$ and $-CH_2$ groups and the rocking vibration of the $-CH_2$ groups.[37] The FTIR spectrum of PW/PCPC is essentially identical to that of pure PW, with no new absorption peaks appearing or observable peak shifts, further confirming the good compatibility between PW and PCPC. These FTIR results are consistent with the XRD analysis.

Differential scanning calorimetry (DSC) measurements revealed the phase change behavior and heat storage capacity of pure PW and all composite PCMs, with the corresponding DSC curves shown in Fig. 3(a). Pure PW exhibits two distinct characteristic peaks during both endothermic and exothermic processes, corresponding to the solid–solid and solid–liquid phase transitions of paraffin, respectively.[38] During the solid–liquid phase transition, pure PW exhibits a melting temperature (T_m) of 53.1 °C with a melting enthalpy (ΔH_m)
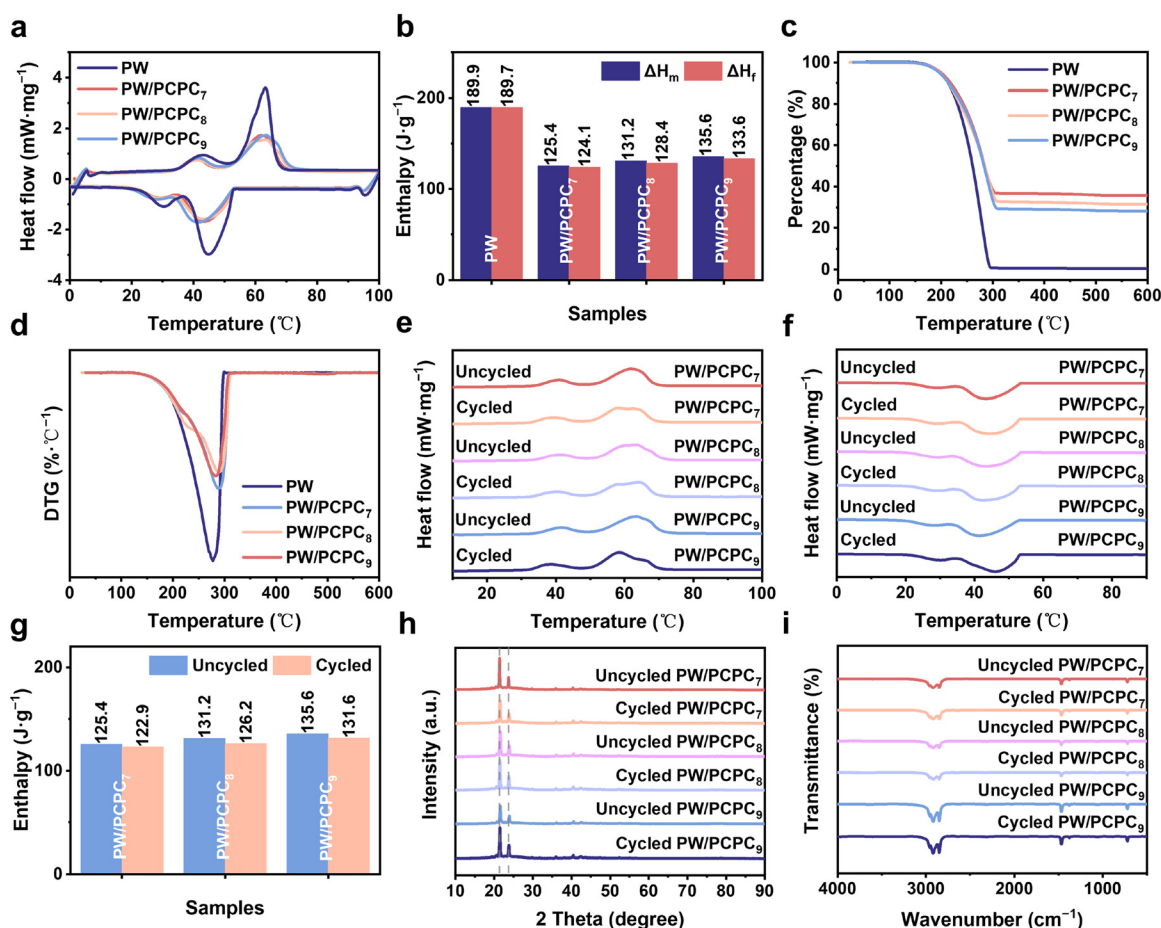
FIG. 3. (a) DSC curves of PW and PW/PCPC. (b) Enthalpy of melting and solidification for PW and PW/PCPC. TGA curves (c) and DTG curves (d) of PW and PW/PCPC. (e) and (f) DSC curves of PW/PCPC before and after thermal cycles. (g) Enthalpy of melting and solidification for PW/PCPC before and after thermal cycles. XRD patterns (h) and FTIR spectrum (i) of PW/PCPC before and after thermal cycles.

of 189.9 J g^{-1}, and a freezing temperature (T$_f$) of 52.7 °C with a freezing enthalpy (ΔH$_f$) of 189.7 J g^{-1}. Compared with pure PW, PW/PCPC shows similar endothermic/exothermic characteristic peaks, with detailed phase change parameters summarized in Fig. 3(b) and Table S2. The reduction in the phase change enthalpy of PW/PCPC is attributed to the nonparticipation of the PCPC encapsulation matrix in the phase transition process.[39] The theoretical encapsulation efficiency of PW in the composite PCMs was calculated using the following equation:

$$\text{Theoretical encapsulation ratio}(\%)$$
$$= \frac{\Delta H_{m,Sample} + \Delta H_{f,Sample}}{\Delta H_{m,PEG} + \Delta H_{f,PEG}} \times 100\%. \quad (1)$$

The theoretical encapsulation rates of PW/PCPC$_7$, PW/PCPC$_8$, and PW/PCPC$_9$ (the ratios of PC to NaCl are 1:7, 1:8, and 1:9, respectively) were calculated to be 65.75%, 68.84%, and 71.13%, respectively, indicating the effective encapsulation capability of the PCPC matrix for PW. In addition, the heterogeneous nucleation effect induced by the PCPC scaffold promoted the crystallization of PW, resulting in a

slight decrease in the composite's T$_m$ to a point below its freezing temperature T$_f$.

The shape stability of PW and PW/PCPC was assessed by placing them on a heating plate at 80 °C. As shown in Fig. S2, PW rapidly melts within 10 min of heating, whereas PW/PCPC maintains a stable shape during the heating process, indicating that PCPC can effectively confine the molten PW. The thermogravimetric analysis (TGA) and derivative thermogravimetry (DTG) curves of PW and PW/PCPC are shown in Figs. 3(c) and 3(d), respectively. As summarized in Table S3, the primary thermal decomposition of the PW/PCPC composite occurred between 130 and 320 °C. The onset decomposition temperature (T$_{onset}$) of PW is slightly higher than that of PW/PCPC, while the peak decomposition temperature (T$_{peak}$) of PW is lower. The results demonstrate that the thermal stability of the PW/PCPC composite for practical applications, as its initial decomposition temperature is significantly higher than its operating temperature (near T$_m$). Furthermore, the actual encapsulation rate of PW/PCPC$_7$, PW/PCPC$_8$, and PW/PCPC$_9$ was determined to be 63.8%, 67.3%, and 70.8%, respectively. The actual encapsulation rate of PW/PCPC is significantly lower than the theoretical encapsulation rate, which confirms the role of PCPC in promoting PW crystallization.

The thermal reliability of the PW/PCPC composite was evaluated by subjecting it to 200 thermal cycles between 0 and 80 °C. The DSC curves of the composite before and after the cycles are compared in Figs. 3(e) and 3(f). As shown in Table S4 and Fig. 3(g), the phase transition performance of PW/PCPC exhibits no significant degradation after the thermal cycling. After thermal cycling, the ΔH_m of PW/PCPC composites was measured to be 122.9, 126.2, and 131.6 J g^{-1}, retaining 98%, 96.2%, and 97.1% of their initial values, respectively. The minimal changes in both T_m and T_f indicate the excellent thermal reliability of the PW/PCPC composite. The XRD pattern [Fig. 3(h)] and FTIR spectrum [Fig. 3(i)] of PW/PCPC remain virtually identical before and after the cycling test. This confirms the structural stability of PW/PCPC throughout the cycling process and demonstrates its reliability for long-term applications.

The light absorption properties of PCMs are a crucial determinant of their efficiency in solar energy harvesting. The optical absorption characteristics of the samples were characterized via UV-Vis absorption spectroscopy. It can be observed that pure PW exhibits

weak light absorption capacity, while the presence of PCPC significantly enhances the light absorption ability of the composite PCMs [Fig. 4(a)]. Furthermore, the carbon skeleton of PCPC remarkably improves the thermal conductivity of PW/PCPC, with the thermal conductivity increasing from 0.298 W m^{-1} K^{-1} for pure PW to a maximum of 0.418 W m^{-1} K^{-1} for PW/PCPC$_7$ [Fig. 4(b)]. However, the thermal conductivity of PW/PCPC decreases slightly as the PW loading increases. First, the increase in porosity of PCPC due to the higher content of the template agent results in a sparse carbon skeleton and a reduction in the number of effective heat transfer pathways. Second, the increase in PW loading significantly disrupts the continuity of the three-dimensional carbon network, causing originally efficient thermal pathways to be fragmented and blocked by the low-thermal-conductivity paraffin. Simultaneously, the introduction of PW increases the number of carbon/PW interfaces, and the extremely high interfacial thermal resistance severely scatters phonons, thereby leading to a decrease in thermal conductivity (Fig. S3). The enhanced light absorption capacity and improved thermal conductivity contribute to
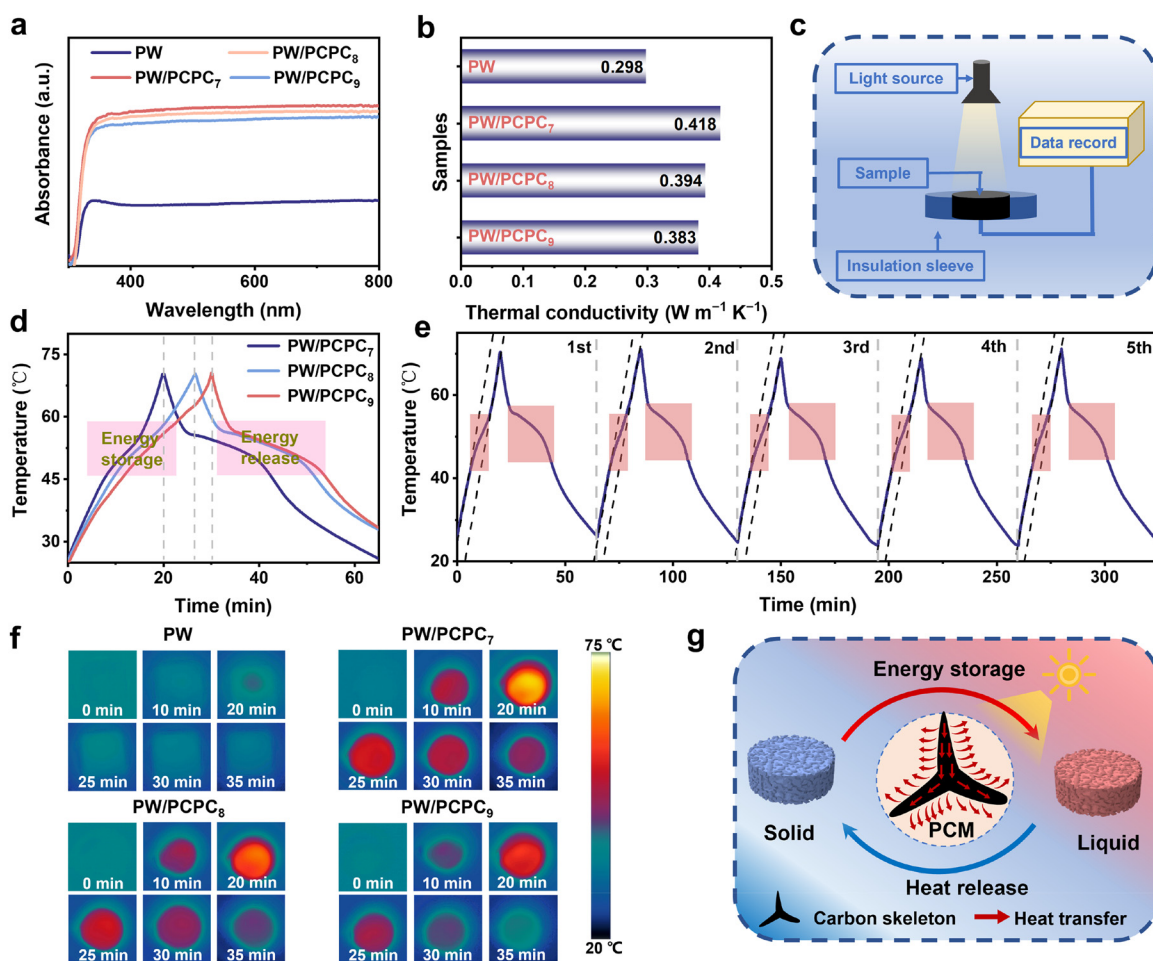

FIG. 4. Absorption spectra (a) and thermal conductivities (b) of PW and PW/PCPC. (c) Solar-thermal energy conversion test system. (d) Temperature change curves of PW/PCPC under 1.0 sun irradiation. (e) Photothermal conversion curves of PW/PCPC$_7$ in five cycles under 1.0 sun irradiation. (f) Infrared thermal images of PW and PW/PCPC. (g) Solar-thermal conversion mechanism diagram of PW/PCPC.

synergistically improving the photothermal conversion and thermal energy storage capabilities of PW/PCPC.

As shown in Fig. 4(c), the photothermal conversion performance of the composite PCMs was evaluated using a self-designed testing setup, which recorded the time–temperature curves under irradiation at 1.0 sun intensity and subsequent light removal. Under illumination, the internal temperature of PW/PCPC increases rapidly, with a brief plateau appearing around 45 °C, corresponding to the melting endotherm process of internal PW. After light removal, the temperature of PW/PCPC gradually decreases, and a distinct slowing plateau emerges around 50 °C, corresponding to the solidification exotherm process of PW [Fig. 4(d)]. Meanwhile, due to the influence of light absorption capacity and thermal conductivity, PW/PCPC$_7$ exhibits a significantly faster heating rate during photothermal conversion than PW/PCPC$_8$ and PW/PCPC$_9$, requiring less time to reach the same temperature. The photothermal conversion efficiency of the composite PCMs was calculated using the following equation:[40]

$$\eta = \frac{m \times \Delta H_m}{P \times S \times \Delta t} \times 100\%, \qquad (2)$$

where m, ΔH_m, P, S, and Δt denote the sample mass, melting enthalpy, light intensity, illuminated area, and phase transition time, respectively. As shown in Fig. S4, taking PW/PCPC$_7$ as an example, the phase transition time was obtained by subtracting the phase change onset time from the phase change completion time using the tangent method. Notably, PW/PCPC$_7$ achieves the highest photothermal conversion efficiency of 89.68% (Fig. S5), exceeding that of many composite PCMs based on biochar and biomass-derived porous carbons (Fig. S6). The composite also demonstrates excellent photothermal cycling stability, as the time–temperature curve of PW/PCPC$_7$ shows no significant change after five cycles [Fig. 4(e)]. Furthermore, an infrared thermal imager was employed to visually compare the photothermal conversion capabilities of pure PW and PW/PCPC composite [Fig. 4(f)]. Under identical illumination conditions, the surface temperature of pure PW remains virtually unchanged, while that of PW/PCPC rises sharply. After light removal, the PW/PCPC composite maintains a relatively high temperature for an extended period due to the release of latent heat during the solidification of PCMs. A schematic diagram illustrating the photothermal conversion mechanism of the composite PCMs is presented in Fig. 4(g). The porous carbon
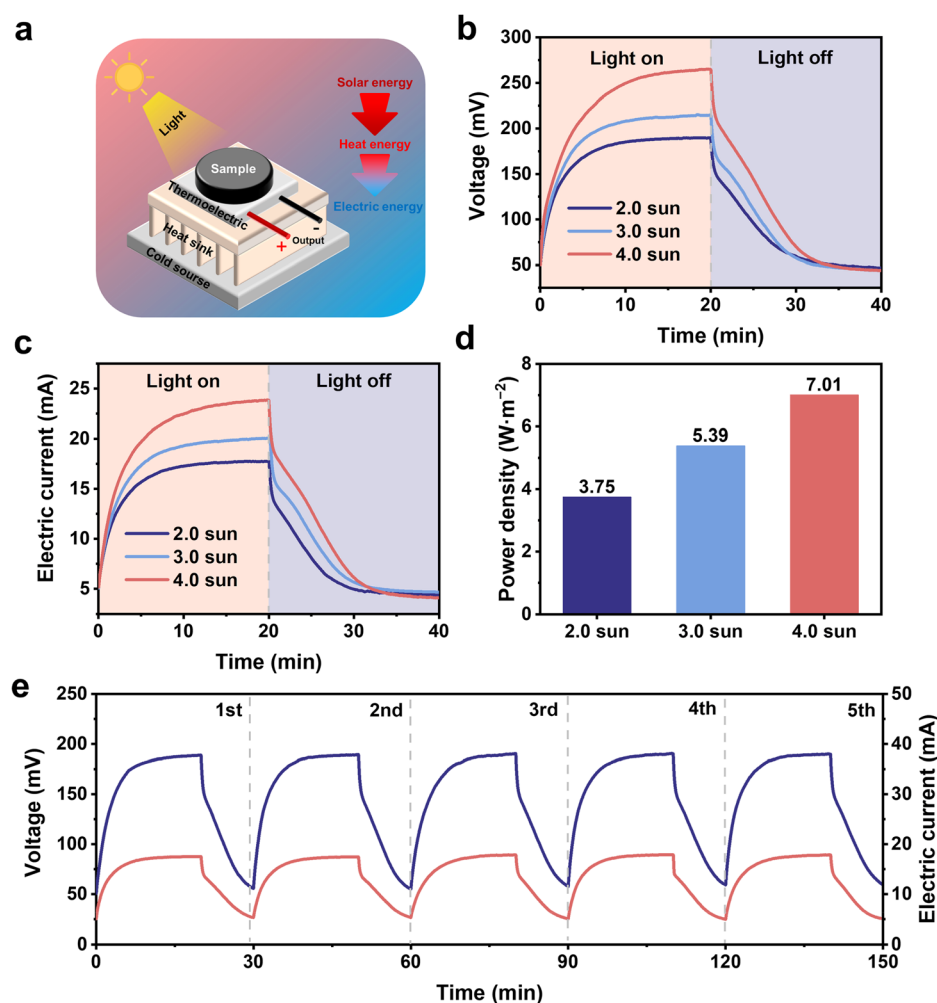

FIG. 5. (a) Schematic diagram of solar-thermal-electricity conversion measurement system. (b) Output power histograms of TES under 2.0, 3.0, and 4.0 sun irradiation. voltage output variation curves (c) and current output variation curves (d) curves under 2.0, 3.0, and 4.0 sun irradiation. (e) Voltage output variation curves and current output variation curves during five cycles under 4.0 sun irradiation.

skeleton, constructed using petroleum coke as the raw material, converts absorbed light energy into thermal energy through molecular thermal vibration under illumination, which is then transferred to the PCM and stored in the form of phase change latent heat. After light removal, the phase change latent heat of the PCM is released in the form of thermal energy, enabling energy storage and utilization.

A solar-thermal-electricity conversion test system was constructed. It comprised the PW/PCPC as the hot end combined with a commercial thermoelectric generator (TEG), while using cold water as the cold source at the bottom to establish a temperature difference across the TEG. This setup aimed to extend the application of PW/PCPC in the field of solar-thermal-electricity conversion [Fig. 5(a)].[41] Due to the excellent photothermal conversion performance, the temperature of PW/PCPC$_7$ hot end rises rapidly under illumination. This creates a significant temperature difference across the TEG, triggering a thermoelectric effect, thereby generating voltage and current. Under 2.0 sun illumination, the device outputs a maximum voltage of 189.8 mV after 20 min. The output voltage exhibits a positive correlation with light intensity, reaching a maximum of 265.1 mV under 4.0 sun illumination [Fig. 5(b)]. The output current follows a similar trend, reaching a maximum of 23.8 mA at 4.0 sun intensity [Fig. 5(c)]. After illumination is turned off, PW/PCPC$_7$ releases the energy stored in the previous photothermal conversion in the form of latent heat from the PW, slowing the temperature drop at the hot end and achieving continuous voltage and current output. Based on the recorded voltage and current, the maximum power density of the device under four times the intensity of sunlight is estimated to be $7.01\,\mathrm{W\,m^{-2}}$ [Fig. 5(d)]. Furthermore, its output performance remained highly stable over five consecutive test cycles [Fig. 5(e)]. These results confirm the high efficiency and excellent cycling stability of the PW/PCPC$_7$-based device for solar-thermal-electricity conversion.

In summary, this work developed a hierarchically porous carbon (PCPC) from the by-product petroleum coke and employed it as a robust scaffold to encapsulate PCM. The abundant pore structure of PCPC enables effective PW encapsulation, yielding a composite PCM with a high latent heat of up to $134.4\,\mathrm{J\,g^{-1}}$. PW/PCPC exhibits outstanding dimensional stability and thermal reliability, showing no signs of leakage over 200 thermal cycles. Leveraging the superior light absorption and enhanced thermal conductivity provided by PCPC, the PW/PCPC composite achieves a remarkable photothermal conversion efficiency of 89.68% at one sun intensity. Furthermore, a proof-of-concept solar-thermal-electricity conversion device integrating PW/PCPC achieved sustained power output with a maximum output power density of $7.01\,\mathrm{W\,m^{-2}}$. This implementation demonstrates the significant potential of PW/PCPC for practical solar energy collection and conversion.

See the supplementary material for the preparation methods, test, and characterization methods of PCPC and PW/PCPC, as well as the relevant supplementary figures and tables.

AUTHOR DECLARATIONS
Conflict of Interest

The authors have no conflicts to disclose.

Author Contributions

Jianhua Bian: Visualization (equal); Writing – original draft (equal). **Lili Wang:** Supervision (equal); Writing – review & editing (equal). **Libing Liao:** Supervision (equal). **Guocheng Lv:** Conceptualization (equal); Project administration (equal).

DATA AVAILABILITY

The data that support the findings of this study are available within the article and its supplementary material.

REFERENCES

[1]G. Wang, Z. Tang, Y. Gao, P. Liu, Y. Li, A. Li, and X. Chen, "Phase change thermal storage materials for interdisciplinary applications," Chem. Rev. **123**(11), 6953–7024 (2023).

[2]W. Wang, M. Zhang, R. Mi, Y. Liu, and J. Chen, "Facile synthesis of porous Co$_3$O$_4$ nanosheets containing abundant oxygen vacancies for boosted lithium-ion storage," J. Alloys Compd. **888**, 161615 (2021).

[3]M. Liu, G. Lv, H. Liu, Y. Fu, J. Zhang, L. Liao, D. Jiang, and J. Guo, "A self-charging aluminum battery enabled by spontaneous disproportionation reaction," Adv. Funct. Mater. **33**(38), 2301913 (2023).

[4]M. Sun, Q. Wang, and H. Di, "A review of lignocellulosic biomass-based shape-stable composite phase change materials," J. Energy Storage **73**, 109114 (2023).

[5]W. Sun, G. Liang, F. Feng, H. He, and Z. Gao, "Study on sodium acetate trihydrate-expand graphite-carbon nanotubes composite phase change materials with enhanced thermal conductivity for waste heat recovery," J. Energy Storage **55**, 105857 (2022).

[6]A. A. M. Omara, "Phase change materials for waste heat recovery in internal combustion engines: A review," J. Energy Storage **44**, 103421 (2021).

[7]B. Singh, R. S. Rai, P. Yadav, S. Srivastava, and C. Yadav, "Application of phase change materials in solar water heating systems—A comprehensive review," Sol. Energy Mater. Sol. Cells **293**, 113888 (2025).

[8]A. C. Bonillo, Y. Lum, J. K. Muiruri, N. Tomczak, W. Wu, S. Wang, W. Thitsartarn, P. Wang, J. C. C. Yeo, J. Xu, Z. Li, X. J. Loh, and Q. Zhu, "State-of-the-art biodegradable polymers and bio-composites for phase change materials," Sustainable Mater. Technol. **46**, e01728 (2025).

[9]Y. Feng, M. Qin, J. Qin, Z. Shen, X. Chen, Y. Li, and R. Che, "Synergistic thermal management and electromagnetic wave absorption in core-sheath phase change composites," Adv. Funct. Mater. e23075 (published online 2025).

[10]V. V. Tyagi, K. Chopra, R. K. Sharma, A. K. Pandey, S. K. Tyagi, M. S. Ahmad, A. Sarı, and R. Kothari, "A comprehensive review on phase change materials for heat storage applications: Development, characterization, thermal and chemical stability," Sol. Energy Mater. Sol. Cells **234**, 111392 (2022).

[11]Y. Luo, F. Zhang, C. Li, and J. Cai, "Biomass-based shape-stable phase change materials supported by garlic peel-derived porous carbon for thermal energy storage," J. Energy Storage **46**, 103929 (2022).

[12]P. K. S. Rathore and S. K. Shukla, "Enhanced thermophysical properties of organic PCM through shape stabilization for thermal energy storage in buildings: A state of the art review," Energy Build. **236**, 110799 (2021).

[13]W. Zhao, W. Liu, and M. Zhang, "Research progress on carbon aerogel composite phase-change energy storage materials," Carbon **244**, 120725 (2025).

[14]K. Soni and N. L. Panwar, "A detailed review on unlocking the potential of porous biocarbon in composite phase change materials for transformative thermal energy storage," J. Energy Storage **114**, 115725 (2025).

[15]L. Wu, Q. Liu, N. Tang, X. Wang, L. Gao, Q. Wang, G. Lv, and L. Hu, "Development of two-dimensional nano Mts/SA phase change materials for self-adjusting temperature of pavement," Constr. Build. Mater. **349**, 128753 (2022).

[16]Y. Feng, G. Hai, G. Sun, K. Chen, X. Wang, J. Zhao, Y. Li, and X. Chen, "Dual-functional phase change composites integrating thermal buffering and electromagnetic wave absorption via multi-interfacial engineering," Adv. Fiber Mater. **7**(6), 1873–1887 (2025).

[17]Y. Li, Y. Feng, M. Qin, K. Chen, Y. An, P. Liu, Y. Jiang, Z. Shen, and X. Chen, "Co-anchored hollow carbonized Kapok fiber encapsulated phase change materials for upgrading photothermal utilization," Small **21**(21), 2500479 (2025).

[18]M. Li and J. Shi, "Review on micropore grade inorganic porous medium based form stable composite phase change materials: Preparation, performance improvement and effects on the properties of cement mortar," Constr. Build. Mater. **194**, 287–310 (2019).

[19]X. Chen, J. Lin, Y. Feng, K. Chen, M. Qin, S. Han, Y. Jiang, Z. Shen, and Y. Li, "Carbon-metal network boosting photon/phonon transport in photothermal phase change materials," Carbon **238**, 120192 (2025).

[20]P. Singh, R. K. Sharma, M. Khalid, R. Goyal, A. Sarı, and V. V. Tyagi, "Evaluation of carbon based-supporting materials for developing form-stable organic phase change materials for thermal energy storage: A review," Sol. Energy Mater. Sol. Cells **246**, 111896 (2022).

[21]B. Zhang, Y. Chen, Y. Mu, B. Yang, X. Li, S. Ke, X. Min, R. Mi, X. Wu, Y. Liu, Z. Huang, and M. Fang, "A novel cobalt-reinforced graphene aerogel composite phase change material with excellent energy storage capacity for low-temperature industrial waste heat recovery," J. Energy Storage **107**, 114920 (2025).

[22]J. Ren, R. Tan, C. Huang, J. Chen, M. Huang, and Q. Zhang, "Self-assembled cellulose nanofibers/graphene aerogel-supported phase change composites with a three-dimensional network structure for enhanced solar-thermal energy conversion and storage," J. Colloid Interface Sci. **700**, 138343 (2025).

[23]L. Zhou, X. Wang, Q. Wu, Z. Ni, K. Zhou, C. Wen, X. Yan, and T. Xie, "Carbon nanotube sponge encapsulated Ag-MWCNTs/PW composite phase change materials with enhanced thermal conductivity, high solar-/electric-thermal energy conversion and storage," J. Energy Storage **84**, 110925 (2024).

[24]L. Chen, R. Zou, W. Xia, Z. Liu, Y. Shang, J. Zhu, Y. Wang, J. Lin, D. Xia, and A. Cao, "Electro- and photodriven phase change composites based on wax-infiltrated carbon nanotube sponges," ACS Nano **6**(12), 10884–10892 (2012).

[25]X.-L. Chang, T. Yan, W.-G. Pan, and L.-W. Wang, "Synergistic enhancement of metal–organic framework-derived hierarchical porous materials towards photothermal conversion and storage properties of phase change materials," Appl. Therm. Eng. **255**, 124046 (2024).

[26]M. Fang, R. He, J. Zhou, H. Fei, and K. Yang, "Thermal conductivity enhancement and shape stability of composite phase change materials using MIL-101(Cr)-NH$_2$/expanded graphite/multi-walled carbon nanotubes," J. Energy Storage **86**, 111244 (2024).

[27]L. Chen, Y. Li, H. Fei, J. Tong, and X. Dai, "Properties regulation and application of biomass carbon based composite phase change materials in thermal energy storage," Sol. Energy **298**, 113680 (2025).

[28]K. Moulakhnif, A. El Majd, M. Ghazoui, H. Ait Ousaleh, A. Faik, S. Sair, and A. El Bouari, "Eco-friendly porous carbon from Capparis waste: A green biomass-derived material for high performance thermal energy storage," Environ. Res. **285**, 122599 (2025).

[29]L. Wang, S. Xuan, S. Chen, W. Mo, L. He, and X. Liu, "Contrasting roles of CO$_2$ activation and N$_2$ pyrolysis in bamboo shoot shell carbon for thermal energy storage," J. Energy Storage **132**, 117768 (2025).

[30]Y. Tian, R. Yang, H. Pan, N. Zheng, and X. Huang, "Biomass-based shape-stabilized phase change materials for thermal energy storage and multiple energy conversion," Nano Energy **133**, 110440 (2025).

[31]E. Jang, S. W. Choi, and K. B. Lee, "Effect of carbonization temperature on the physical properties and CO$_2$ adsorption behavior of petroleum coke-derived porous carbon," Fuel **248**, 85–92 (2019).

[32]M. Malekshahian and J. M. Hill, "Effect of pyrolysis and CO$_2$ gasification pressure on the surface area and pore size distribution of petroleum coke," Energy Fuels **25**(11), 5250–5256 (2011).

[33]S. Duan, X. Wu, K. Zeng, T. Tao, Z. Huang, M. Fang, Y. Liu, and X. Min, "Simple routes from natural graphite to graphite foams: Preparation, structure and properties," Carbon **159**, 527–541 (2020).

[34]D. Gowthami and R. K. Sharma, "Influence of hydrophilic and hydrophobic modification of the porous matrix on the thermal performance of form stable phase change materials: A review," Renewable Sustainable Energy Rev. **185**, 113642 (2023).

[35]J. Feng, X. Liu, F. Lin, S. Duan, K. Zeng, X. Bai, X. Wu, Z. Huang, and X. Min, "Aligned channel Gelatin@nanoGraphite aerogel supported form-stable phase change materials for solar-thermal energy conversion and storage," Carbon **201**, 756–764 (2023).

[36]H. Wang, Y. Deng, F. Wu, X. Dai, W. Wang, Y. Mai, Y. Gu, and Y. Liu, "Effect of dopamine-modified expanded vermiculite on phase change behavior and heat storage characteristic of polyethylene glycol," Chem. Eng. J. **415**, 128992 (2021).

[37]A. R. Akhiani, H. S. Cornelis Metselaar, B. C. Ang, M. Mehrali, and M. Mehrali, "MXene/rGO grafted sponge with an integrated hydrophobic structure towards light-driven phase change composites," Composites Part B **264**, 110885 (2023).

[38]H. He, M. Dong, Q. Wang, J. Zhang, Q. Feng, Q. Wei, and Y. Cai, "A multifunctional carbon-base phase change composite inspired by 'fruit growth'," Carbon **205**, 499–509 (2023).

[39]H. Wei and X. Li, "Preparation and characterization of a lauric-myristic-stearic acid/Al$_2$O$_3$-loaded expanded vermiculite composite phase change material with enhanced thermal conductivity," Sol. Energy Mater. Sol. Cells **166**, 1–8 (2017).

[40]X. Guan, B. Song, Y. Liu, H. Zhang, D. Qi, Q. Gou, R. Gao, C. Zhao, and A. Li, "Photothermal conversion-driven thermal conductivity and energy storage synergistic enhancement in hierarchical porous N-doped biochar-based phase change materials," Energy **338**, 138722 (2025).

[41]C. Shu, H.-Y. Zhao, X.-H. Lu, P. Min, Y. Zhang, Q. Wang, X. Li, and Z.-Z. Yu, "High-quality anisotropic graphene aerogels and their thermally conductive phase change composites for efficient solar–thermal–electrical energy conversion," ACS Sustainable Chem. Eng. **11**(32), 11991–12003 (2023).